Acoustic characterization of drop impact regimes on a heated surface

Volfango Bertola[1*]
[1]Laboratory of Technical Physics, School of Engineering, University of Liverpool, Liverpool L69 3GH, United Kingdom
*Corresponding author: Volfango.Bertola@liverpool.ac.uk

Abstract
The sound generated by the impact of water drops on heated surfaces is studied experimentally, with the purpose to identify the sound features characteristic of the various impact morphologies. Whilst the sound of drops impacting on liquid surfaces has been investigated extensively, little attention was given to the sound of drops on solid, heated surfaces. The identification of sound features specific to different impact morphologies would enable the impact regime recognition without the need of high-speed imaging visual inspection, and can be used to train machine learning algorithms for automatic impact regime detection. Water drops were generated from a hypodermic needle suspended above a polished aluminium surface at temperatures between 100°C and 400°C, with impact Weber numbers ranging from 30 to 150. The sound generated upon impact was captured by a supercardioid condenser microphone, and compared with high-speed video recordings of the the impact. Results suggest different impact morphologies generate a sound with distinctive spectral features.

Introduction
The phenomenology of liquid drops impacting on heated surfaces is characterized by a close interplay of hydrodynamics with different heat transfer modes, under large spatial and temporal gradients of the state variables [1,2]. After impact, the drop spreads on the heated surface in a short lapse of time (typically a few milliseconds in case of drops of millimetric size), increasing the area exposed to heat transfer. This induces a heat transfer regime that can be related to the well-known boiling curve [3]. In particular, one can observe: (i) convection heat transfer for surface temperatures below the boiling point of the liquid; (ii) nucleate boiling for surface temperatures just above the boiling point; (iii) film boiling, observed above the critical heat flux (CHF), where the drop is separated from the surface by a vapor layer and (iv) transitional boiling, where the said vapor layer is unstable and the liquid may locally get into contact with the surface. However, the association between heat transfer and impact regimes is not always straightforward, and consequently the classification of impact regimes is still somewhat controversial. To rationalize the rich variety of impact morphologies observed for Newtonian drops impinging on heated surfaces, it was proposed to identify simple impact regimes, displaying one distinctive feature (deposition, rebound, splashing/breakup) and mixed regimes, resulting from the combination of simple regimes with secondary atomization [4]. Such unifying classification, on one hand, embraces the different impact morphologies reported in the existing literature, and on the other hand is simple enough to be used for practical purposes.
The generation of sound associated with drop impact phenomena, on either solid or liquid surfaces, has been studied for a long time. In 1919, Mallock observed the impact of liquid drops produced sounds of the same class of sounds produced by the impact of solid spheres [5]. Franz [6] discussed several mechanisms of noise production by impacting drops and solids, and seems to have been the first one to speculate an air bubble can be entrained in the water, and that the sound energy radiated by an individual bubble is often greater than the sound energy radiated by the impact of the water droplet. Most investigations focused on the underwater noise generated by rain, a phenomenon initially reported by Knudsen et al. [7]. These studies were motivated both by the military need for a better understanding of the natural mechanisms of underwater noise generation, and by the development of acoustical techniques to probe geophysical phenomena [8,9].
The first attempts to characterise rain noise spectra were jeopardised by the inability to obtain reliable data beyond 10 kHz [10-12]. Later on, data obtained over a much broader frequency range enabled an accurate identification of the unique acoustic signature of rain [13-16]. The combination of sound measurements with high-speed imaging led to the conclusion that the sound generated during drop impact is unequivocally associated to the entrainment of air bubbles into the liquid [17-19]. Specifically, it was observed that the impact itself produced an acoustic signal indistinguishable from the electronic noise, while the bubble noise was very strong, and corresponds to a peak at 14 kHz in the frequency spectrum [20,21]. However, the range of parameters (impact velocity, drop diameter, fluid properties) where bubble entrainment is observed is usually narrow [18], and for high energy impacts a different bubble formation mechanism generates sound below 10 kHz [22].
When a drop collides with a solid surface, depending on the surface temperature and on the impact kinetic energy one can observe a significant amount of vapour bubbles and/or capillary breakup events, which constitute a well-known source of noise. However, the literature does not report any systematic investigations of the sound generated by drops impacting on heated surfaces. Recently, the emission of sound emitted by a drop of water gently deposited on a substrate with a temperature much higher than the boiling point of water (Leidenfrost drop) was investigated experimentally [23]. In this case, periodic beats due to non-uniform evaporation in the gap between the liquid drop and the surface were recorded and analysed using Fourier and wavelet transforms.

In the present work, it is proposed to identify different impact morphologies based on their acoustic footprint. In particular, the noise generated during drop impact is strongly dependent on the number, the size, and the evolution of vapor bubbles hence it exhibits distinctive features for each impact morphology. Currently, the identification of drop impact regimes is carried out using high speed imaging, however this requires expensive equipment and optical access to the system, which is often difficult or impossible in critical areas of industrial systems. The identification of sound features specific to different impact morphologies would enable the impact regime recognition without the need of high-speed imaging visual inspection, and can be used to train machine learning algorithms for automatic impact regime detection.
The noise of drop impact was recorded using a supercardioid condenser microphone placed near the target surface and synchronized with a high-speed camera, for different surface temperatures and different impact Weber numbers. The recorded sound tracks corresponding to each experimental condition were analyzed and compared with the high-speed videos to identify the distinctive spectral features of each impact morphology.

Material and methods

Experimental setup

The experimental setup is displayed in Figure 1. De-ionised water drops (equilibrium diameter $D_0 \approx 3$ mm) were created at the tip of a blunt hypodermic needle (i.d. 0.495 mm - gauge 21) by a screw-driven syringe dispenser, and detached under their own weight. In order to change the impact velocity, the dropping height was adjusted using a digital height gauge with a precision of ± 0.05 mm. The needle was positioned above the surface of an aluminium square block (40×40 mm) containing two electric cartridge heaters (100 W each) symmetric with respect to the point of impact to ensure a uniform temperature field. The surface was mirror polished with a chemical abrasive. Temperature was controlled within $\pm 1^{\circ}$C by a PID controller driven by a K-thermocouple placed 1 mm below the point of impact.
A high-frame rate CMOS camera (Mikrotron MC1310) equipped with a 18–108/2.5 macro zoom lens (Navitar Zoom 7000) and horizontally aligned with the surface recorded the impacts of single drops. Back-to-front illumination was provided by a LED diffuse backlight (Advanced Illumination) which ensured a uniform illumination intensity, and images with a resolution of 400×400 pixels were captured at 1000 frames per second. Magnification was kept constant throughout all experiments and lengths on the image could be calculated by comparison with a reference length (typical spatial resolution: 35 pixels/mm). To ensure a fine optical alignment, the camera, the heated surface and the backlight were fixed to an optical breadboard.

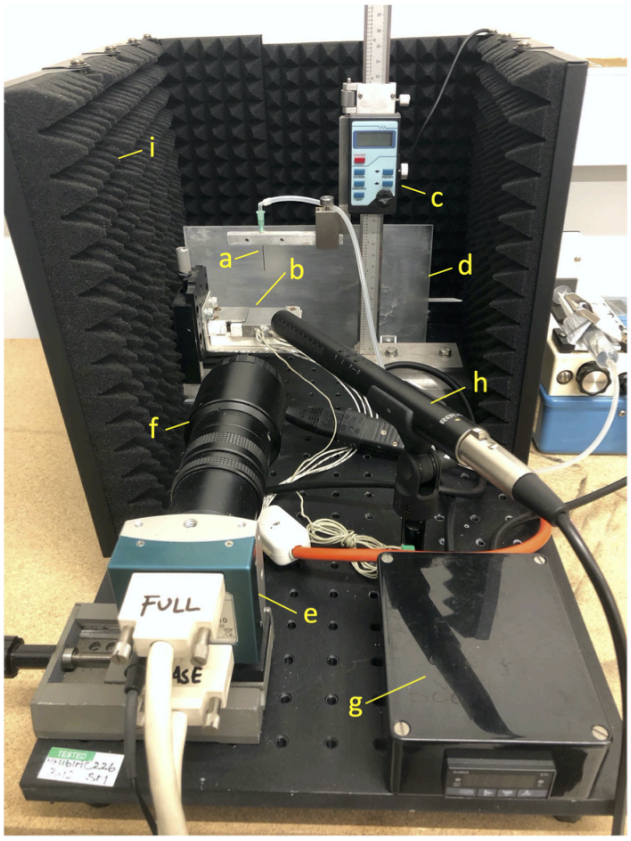

Figure 1. Experimental kit: (a) dispensing needle; (b) target surface; (c) height gauge; (d) light diffuser; (e) high-speed camera; (f) zoom lens; (g) PID temperature controller; (h) directional condenser microphone; (i) sound absorbing shield.

The noise generated by drop impacts was captured by a supercardioid condenser microphone (Røde NTG4+) placed above the impact surface at a distance of a few centimeters from the point of impact, and converted into a 16-bit digital waveform sampled at 44.1 kHz. The drop dispensing system the target surface and the microphone sensor were surrounded on three sides by an acoustic foam isolation shield.

Procedure

Drop impacts were recorded for impact Weber numbers, $We = \rho U_{imp}^2 D_0/\sigma$, between 20 and 160, and surface temperatures between 100°C and 400°C, to cover all of the impact morphologies identified previously [4]. The location of experimental points on the impact regime map is displayed in Figure 2. For each set of experimental parameters (i.e., surface temperature and Weber number), the impact experiment was repeated five times for the sake of statistical analysis.

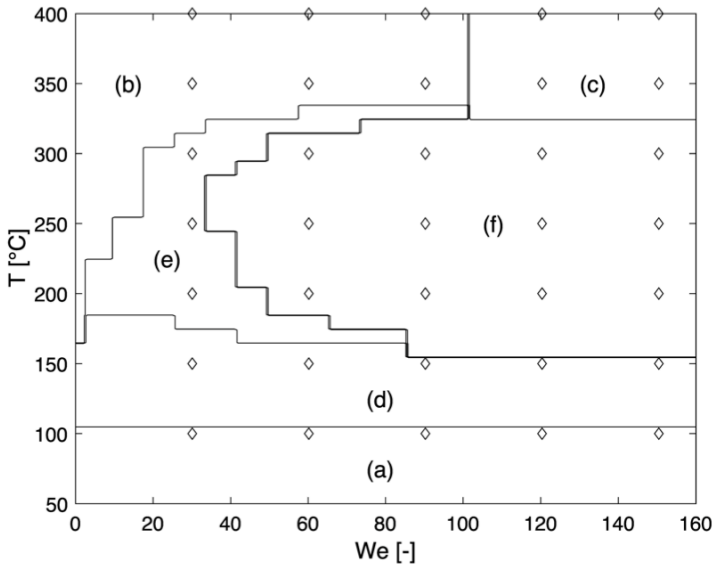

Figure 2. Location of experimental points (⋄) on the impact regime map [4]: (a) deposition; (b) dry rebound; (c) breakup; (d) deposition with secondary atomisation; (e) rebound with secondary atomisation; (f) breakup with secondary atomisation.

The digital videos of impacting droplets were processed by subtracting the background and by adjusting the image brightness, contrast, gamma correction and digital gain in order to highlight small satellite droplets.
The audio waveforms were pre-processed by trimming down to a duration of 5 s, and by applying a noise reduction filter with sensitivity of 5 dB and reduction magnitude of 30 dB (TechSmith Camtasia). To isolate the sound generation due to the first impact from the sound due to subsequent events, the waveform length was further reduced to a duration of 1 s. The pre-processed waveforms were then detrended by subtracting the average before computing their power spectral density using a Blackman windowing, as well as the time-frequency spectrogram [24].

Results and discussion

Figure 3 displays the six impact morphologies observed (described above), along with the corresponding sound waveform plotted in the time domain. For simple drop deposition (Figure 3a), the sound intensity is extremely weak, and the impact event at t ≈ 2.5 s can be barely distinguished from the background noise, because the fluid is not boiling. The waveform recorded in case of dry rebound (Figure 3b) shows an impulsive amplitude spike corresponding to drop impact at t ≈ 0.8 s, a second spike of smaller amplitude corresponding to the drop-surface contact after the first rebound at t ≈ 1.5 s, and finally damped oscillations starting at t ≈ 2 s, which correspond to the boiling liquid deposited on the surface after the second rebound. In the case of drop breakup (Figure 3c), the amplitude spike corresponding to impact at t ≈ 1.9 s is followed by growing oscillations due to the boiling in smaller satellite droplets; the large amplitude oscillations at t ≈ 3.3 s correspond to the final boiling in the residual liquid drop when the vapour film that separates it from the surface collapses. When the surface temperature is sufficiently high to cause boiling after drop deposition, secondary atomisation is observed due to bursting of vapour bubbles on the drop surface (Figure 3d). In this case, the sound waveform shows large oscillations initially of nearly constant amplitude starting at t ≈ 1.7 s, which rapidly decay as the drop evaporates completely. The waveform generated by a drop impact with secondary atomisation (Figure 3e) is very similar to that generated by a dry rebound (Figure 3b), with a large amplitude spike corresponding to the first impact. Finally, drop breakup with secondary atomisation (Figure 3f) also generates a large amplitude spike, immediately followed by oscllations due to the generation of satellite droplets, however of smaller amplitude with respect to the case of satellite droplets generated after drop deposition (Figure 3d).

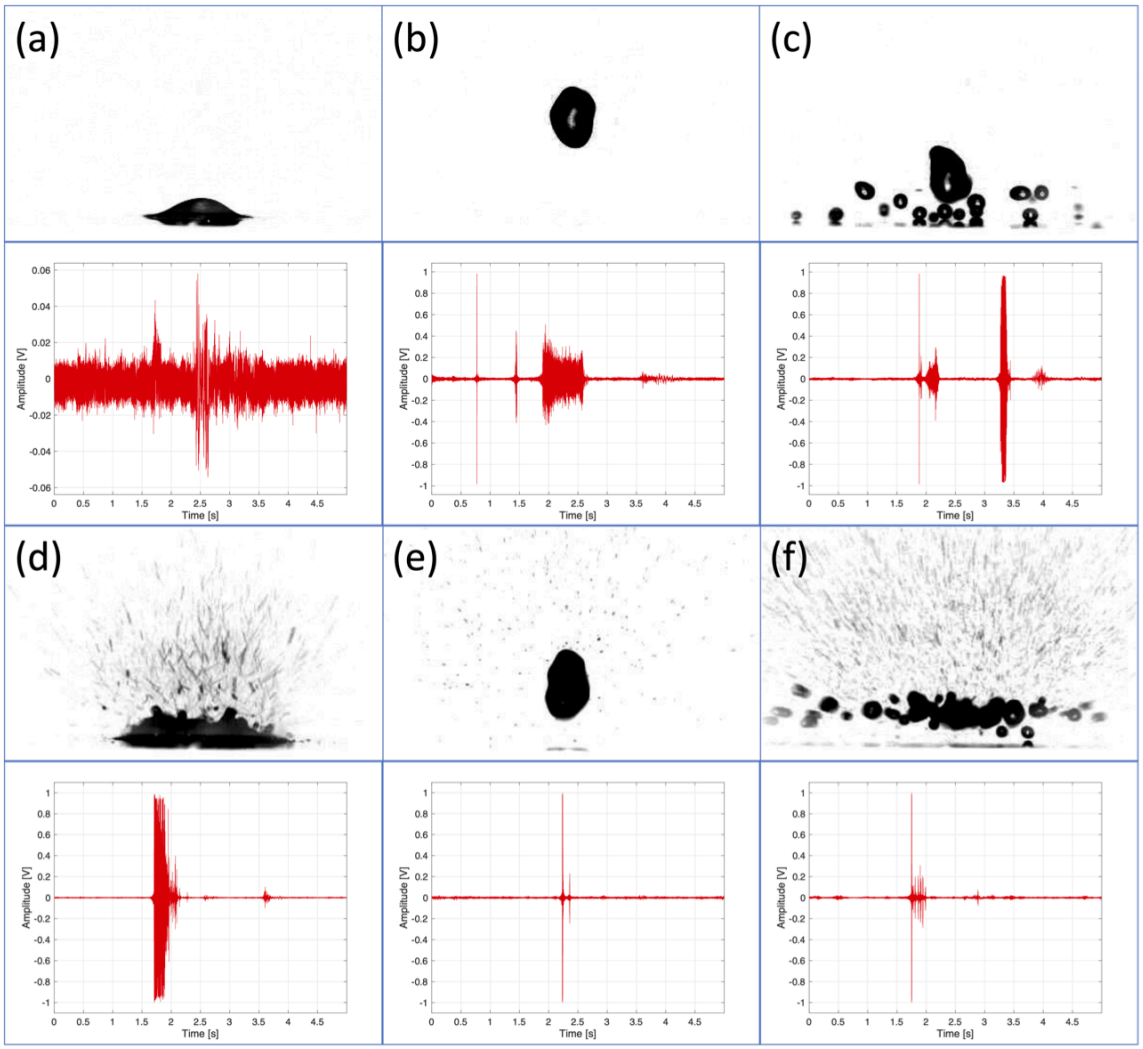

Figure 3. Drop impact morphologies and corresponding audio waveform in the time domain: (a) deposition (T = 100°C, We = 90); (b) dry rebound (T = 400°C, We = 60); (c) breakup (T = 350°C, We = 150); (d) secondary atomisation (boiling, T = 150°C, We = 60); (e) rebound with secondary atomisation (T = 250°C, We = 30); (f) breakup with secondary atomisation (T = 25°C, We = 120).

Figures 4 - 9 display the spectral analysis of the sound waveforms described qualitatively above. In the case of simple drop deposition without boiling (Figure 4), the power density spectrum has a maximum at 0 Hz representing the white noise background. One can observe a very weak ripple around 600 Hz, which represents the impact event recorded in the corresponding oscillogram (Figure 3a) at t ≈ 2.5 s. However, the waveform amplitude and the signal to noise ratio are too small to enable univocal conclusions.

For a drop bouncing on the surface without emission of secondary atomisation (dry rebound), the power density spectrum exhibits one dominant characteristic frequency around 20 kHz, as shown in Figure 5a. As expected, the time-frequency spectrogram (Figure 5b) indicates the sound generation occurs as a single high-frequency pulse, corresponding to the spike in the oscillogram (Figure 3b).

The drop breakup power density spectrum, displayed in Figure 6a, exhibits a clear maximum at a frequency around 11 kHz, and at least three more characteristic frequencies at 15 kHz, 6 kHz, and 3 kHz, in decreasing order of spectral power density. The corresponding time-frequency spectrogram, shown in Figure 6b, suggests the highest frequency is associated with the impact event shortly after t ≈ 0.3 s, while the lower frequencies appear at t ≈ 0.4 s, when breakup occurs as the impacting drop approaches maximum spreading.

In the case of secondary atomisation due to contact boiling and the subsequent bubble bursting on the drop surface, the dominant characteristic frequency is around 6 kHz, about one half of the characteristic frequency of drop breakup (Figure 7a). One can observe other characteristic frequencies of smaller spectral power density at 9 kHz, 12 kHz, and 3 kHz. The corresponding time-frequency spectrogram (Figure 7b), suggests all characteristic frequencies are generated simultaneously upon drop impact (t ≈ 0.2 s), but the higher frequencies fade shortly after.

The power density spectrum of the waveform generated by a drop that rebounds producing secondary atomisation displays only two characteristic frequencies at 15 kHz and 9 kHz, respectively, as shown in Figure 8a. Similar to the

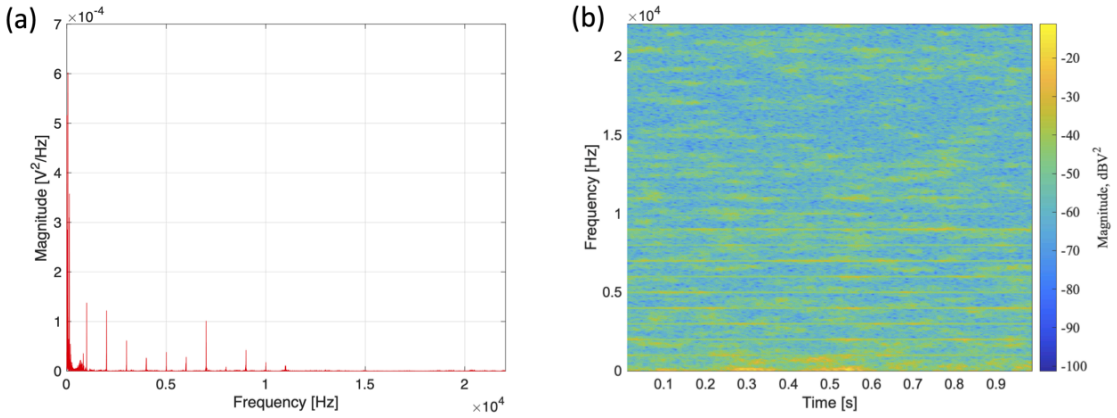

Figure 4. Spectral characterisation of the audio waveform for a drop impact resulting into breakup (T = 100°C, We = 90); (a) power spectral density (periodogram); (b) time-frequency spectrogram.

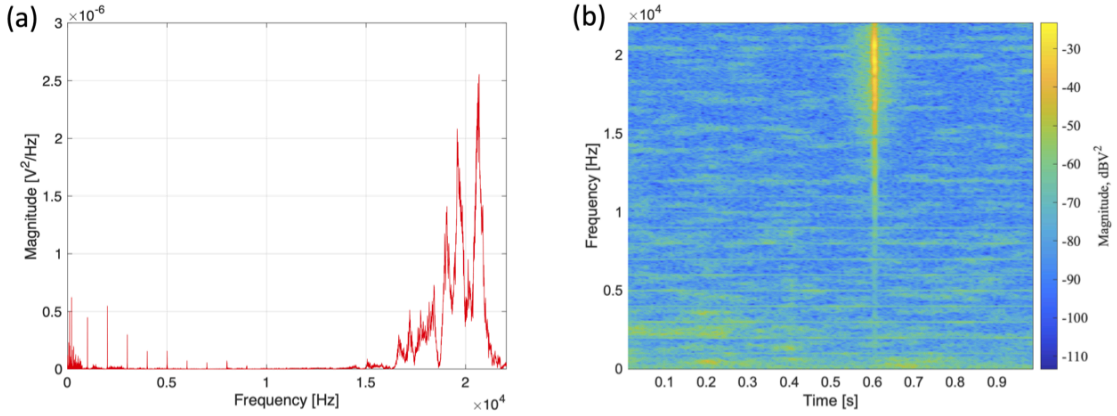

Figure 5. Spectral characterisation of the audio waveform for a drop impact resulting into dry rebound (T = 400°C, We = 60); (a) power spectral density (periodogram); (b) time-frequency spectrogram.

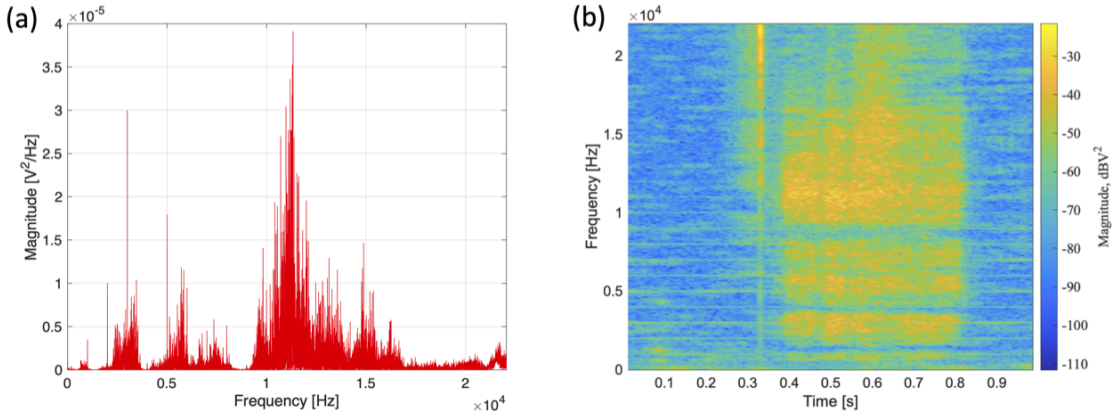

Figure 6. Spectral characterisation of the audio waveform for a drop impact resulting into breakup (T = 350°C, We = 150); (a) power spectral density (periodogram); (b) time-frequency spectrogram.

case of secondary atomisation upon deposition, the time-frequency spectrogram, indicates the two characteristic frequencies are generated simultaneously upon drop impact (t ≈ 0.7 s), as shown in Figure 8b. However, these frequencies are not generated continuously, but as three separate pulses at t ≈ 0.7 s, t ≈ 0.75 s and t ≈ 0.8 s, respectively.

Finally, for a drop breakup with simultaneous emission of secondary atomisation the power density spectrum exhibits one dominant characteristic frequency around 12 kHz, plus two additional characteristic frequencies at 15 kHz and

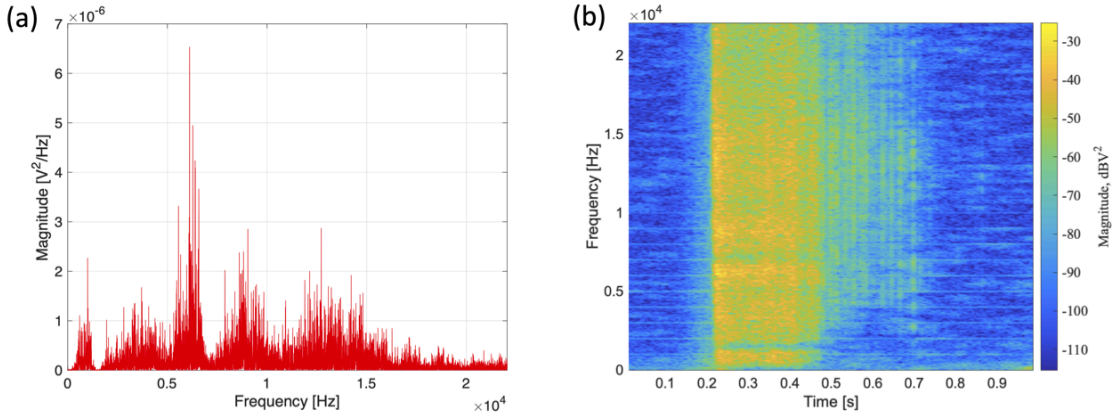

Figure 7. Spectral characterisation of the audio waveform for a drop impact resulting into secondary atomisation (T = 150°C, We = 60); (a) power spectral density (periodogram); (b) time-frequency spectrogram.

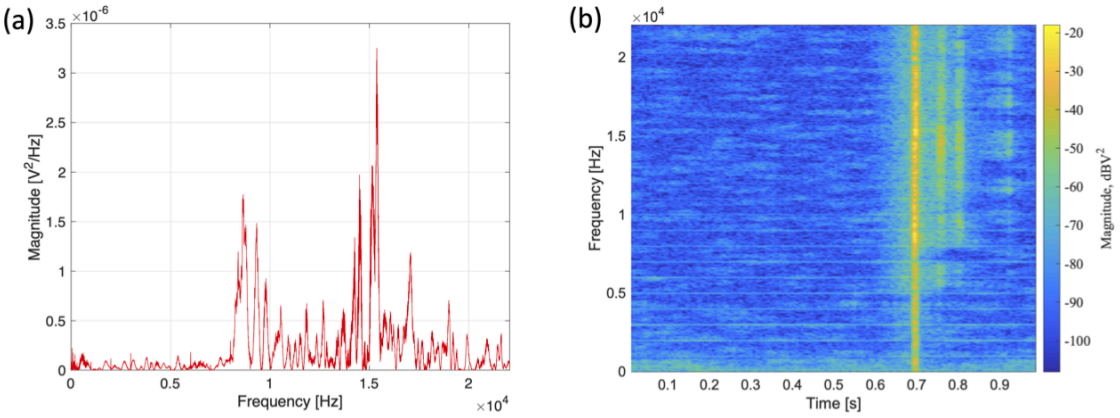

Figure 8. Spectral characterisation of the audio waveform for a drop impact resulting into rebound with secondary atomisation (T = 250°C, We = 30); (a) power spectral density (periodogram); (b) time-frequency spectrogram.

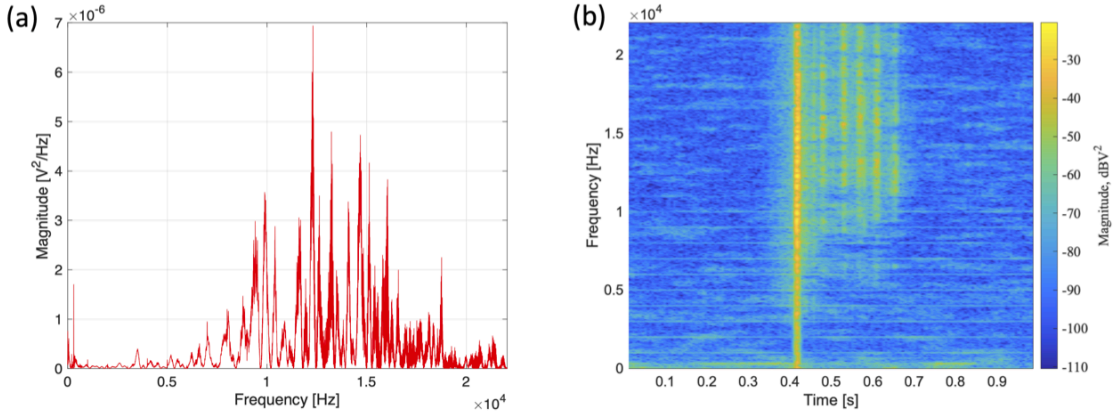

Figure 9. Spectral characterisation of the audio waveform for a drop impact resulting into breakup with secondary atomisation (T = 250°C, We = 120); (a) power spectral density (periodogram); (b) time-frequency spectrogram.

12 kHz, respectively, as shown in Figure 9a. Similar to the case of rebound with secondary atomisation, one can observe several pulses of sound generation at regular time intervals of approximately 0.05 s in the time-frequency spectrogram (Figure 9b).

The characteristic frequencies observed for each drop impact morphology are summarised in Table 1. The sound generated upon dry rebound, which is likely due to the collapse of a single bubble nucleating upon contact with the superheated surface, has a characteristic frequency of about 20 kHz, almost twice the frequency of the sound

generated by drop breakup (approximately 11 kHz), which is governed by capillarity. A similar behaviour was observed for drop impact on liquid surfaces, where the characteristic frequency of the sound depends on the physical mechanism of bubble formation [22].
Simple secondary atomisation due to contact boiling after drop deposition generates a sound with a much lower characteristic frequency of about 6 kHz. Interestingly, the power density spectrum displays other peaks of smaller magnitude at frequencies multiple of 3 kHz, which at present is not understood.
When secondary atomisation occurs simultaneously to either drop rebound or drop breakup, the power density spectrum of the sound generated during drop impact exhibits additional harmonics at lower frequencies. In addition, the analysis of time-frequency spectrograms indicates the sound intensity is not uniform in time but has periodic pulses (beats), which are likely the result of constructive/destructive interference between acoustic waves generated by different physical mechanisms.

Table 1. Characteristic frequencies (kHz) of the sound generated during drop impact for the different impact morphologies. In boldface, the frequency with maximum power spectral density.

	F_I	F_{II}	F_{III}	F_{IV}	F_V	F_{VI}
Deposition	-	-	-	-	-	-
Dry rebound	-	-	-	-	-	**20**
Breakup	3	6	-	**11**	15	-
Secondary atomisation	3	**6**	9	12	-	-
Rebound with secondary atomisation	-	-	9	-	**15**	-
Breakup with secondary atomisation	-	-	10	**12**	15	-

Conclusions

A systematic analysis of the sound generated during drop impact on a heated surface enables the identification of quantitative features associated with the different impact morphologies. In particular, the spectral analysis of sound waveforms reveals the characteristic frequencies of sound generated by drop rebound, by drop breakup, and by the emission of satellite droplets, respectively.
The characteristic frequency of the sound generated by drop rebound is about twice that of the sound generated by drop impact, while the sound of secondary atomisation exhibits multiple characteristic frequencies of lower magnitude. These results suggest there is a potential to identify drop impact morphologies based on acoustic diagnostic techniques, without the aid of high-speed imaging, even in applications where optical access is not feasible. In addition, sound waveforms and/or their power spectra could be used as input data to train machine learning algorithms for automatic impact regime detection.

Nomenclature

D_0	Drop equilibrium diameter [m]
F	Frequency [Hz]
T	Temperature [$^\circ$C]
t	Time [s]
U_{imp}	Impact velocity [m/s]
We	Weber number [-]
ρ	Density [kg/m^3]
σ	Surface tension [N/m]

References

[1] Rein, M., 1993, *Fluid Dynamics Research*, 12, pp. 61-93.
[2] Rein, M., 2003, “Drop–surface interactions”. Springer.
[3] Fujimoto, H., Oku, Y., Ogihara, T., Takuda,H., 2010, *International Journal of Multiphase Flow*, 36, pp. 620-642.
[4] Bertola, V., 2015, *International Journal of Heat and Mass Transfer*, 85, pp. 430-437.
[5] Mallock, A., 1919, *Proc. R. Soc. London Set. A*, 95, pp. 138-143.
[6] Franz, G. J., 1959, *J. Acoust. Soc. Am.*, 31, pp. 1080-1096.
[7] Knudsen,V. O., Alford, R. S., Emling, J. W., 1948, *J. Mar. Res.*, 7, pp. 410-429.
[8] Shaw, P. T., Watts, D. R., Rossby, H. T. 1978, *J. Deep-Sea Res.*, 25, pp. 1225-1233.
[9] Lemon, D. D., Farmer, D. M., Watts, D. R. 1984, *J. Geophys. Res.*, 89, pp. 3462-3472.
[10] Heindsmann, T. E., Smith, R. H., Arneson, A. D. 1955, *J. Acoust. Soc. Am.*, 27, pp. 378-379.
[11] Wenz,G. M. 1962, *J. Acoust. Soc. Am.*, 34, pp. 1936-1956.
[12] Bom, N. 1969, *J. Acoust. Soc. Am.*, 45, pp. 150-156.
[13] Nystuen, J. A. 1986, *J. Acoust. Soc. Am.*, 79, pp. 972-982.
[14] Scrimger, J. A. 1985, *Nature*, 318, pp. 647-649.

[15] Scrimger, J. A., Evans, D. J., McBean,G. A., Farmer, D. M., Kerman, B. R. 1987, *J. Acoust. Soc. Am.*, 81, pp. 79-86.
[16] Scrimger, J. A., Evans, D. J., Yee, W.1989, *J. Acoust. Soc. Am.*, 85, pp. 726-731.
[17] Pumphrey, H. C., Walton, A. J. 1988, *Eur. J. Phys.*, 9, pp. 225-231.
[18] Pumphrey, H. C., Crum, L. A., Bjønø, L. 1989, *J. Acoust. Soc. Am.*, 85, pp. 1518-1526.
[19] Pumphrey, H. C., Elmore, P. A. 1990, *J. Fluid Mech.*, 220, pp. 539-567.
[20] Prosperetti, A., Pumphrey, H. C., Crum, L.A. 1989, *J. Geophys. Res.*, 94, pp. 3255-3259.
[21] Oğuz, H. N., Prosperetti, A., 1990, *J. Fluid Mech.*, 219, pp. 143-179.
[22] Prosperetti, A., Oğuz, H. N. 1993, *Annu. Rev. Fluid Mech.*, 25, pp. 577-602.
[23] Singla, T., Rivera, M., 2020. *Physical Review Fluids*, 5, 113604.
[24] Zhivomirov, H., 2023, Sound Analysis with Matlab, `https://www.mathworks.com/matlabcentral/fileexchange/38837-sound-analysis-with-matlab` ([cit. 2023-05-01]).